

Preparation, degradation and antibacterial properties of Ag₃PO₄/CeO₂

J. H. Feng, S. Y. Li^{*}, W. H. He, H. Tang

School of Chemistry and Bioengineering, Hechi University, Hechi 546300, Guangxi Province, China.

Ag₃PO₄/CeO₂ composites were synthesized with loading Ag source on CeO₂ which was prepared by calcination by one-step precipitation. The structure of Ag₃PO₄/CeO₂ material was characterized and analyzed by different testing methods. At the same time, the degradation effect of the material on the simulated organic pollutant Rhodamine B and the antibacterial effect of the material on *E. coli* were investigated by antibacterial growth curve, colony number and other experiments. The experimental results showed that the degradation rate on 30 mL 40 mg/L Rhodamine B solution by Ag₃PO₄/CeO₂ composites was 99.91 %, which was 6.34 times and 1.67 times that of CeO₂ and Ag₃PO₄, respectively. The order of antibacterial activity of different materials was: Ag₃PO₄/CeO₂ > Ag₃PO₄ > CeO₂. Combined with the photocatalytic free radical quenching experiment, Ag₃PO₄/CeO₂ mainly produced h⁺ and ·O₂⁻ in the degradation process, and photocatalytic materials could produce reactive oxygen species (ROS) and corresponding metal ions during the antibacterial process, and released them to attack the cell wall of *E. coli*, resulting cytoplasm leakage, and thus leading to cell apoptosis.

(Received December 30, 2024; Accepted March 25, 2025)

Keywords: Ag₃PO₄/CeO₂, Degradation, Bacteriostasis

1. Introduction

Photocatalytic technology was a kind of green environmental protection technology for organic pollution degradation and water purification and disinfection. As a relatively new advanced oxidation technology, it had great advantages in environmental governance due to its high efficiency and green sustainability [1-2]. Photocatalytic technology relied on the development of photocatalytic materials. In the solar spectral energy distribution, ultraviolet light with a wavelength of less than 400 nm accounted for only 4 %, while visible light with a wavelength of 400-800 nm accounted for 53%. Therefore, in order to effectively utilize sunlight, it was very important to develop photocatalytic materials with excellent response to visible light [2]. At the same time, the prevalence of pathogenic bacteria and antibiotic resistance posed a great threat to human health, and the development of safe, efficient and low-cost antibacterial agents had become a trend. In recent years, researchers have carried out some research on a variety of antibacterial materials-natural, organic and inorganic substances [3-5]. The development of nanotechnology has made a breakthrough in the

* Corresponding author: lishengying05@163.com
<https://doi.org/10.15251/DJNB.2025.201.341>

development of antibacterial agents. Some photocatalytic-based materials, such as TiO_2 and ZnO , had attracted great attention due to their excellent antibacterial properties. They were considered to be promising antibacterial agents and were expected to be developed into potential broad-spectrum antibacterial agents to replace traditional antibiotics aiming to solve the problem of drug resistance [4-5]. Photocatalytic composite materials had attracted much attention due to their excellent physical and chemical properties and multiple functions. Their physical and chemical properties were different due to their different compositions. Reasonable design could achieve functional diversity [6-7]. Therefore, the design and construction of new catalytic materials with wide spectral response photocatalytic and antibacterial activity was a research hotspot in this field.

In recent years, CeO_2 had attracted much attention in the field of photocatalysis due to its outstanding characteristics such as low cost, environmental friendliness and good oxidation ability [8-9]. While, CeO_2 as a photocatalytic material had good redox ability, a large number of oxygen vacancy defects and high oxygen storage capacity [10-11]. However, CeO_2 still had a wide band gap in practical applications, and it only responded to high-energy ultraviolet light. The high mobility of oxygen active sites and the partial conversion of Ce^{4+} to Ce^{3+} lead to the possible reduction of photocatalytic activity as a carrier. Problems such as oxidation vacancies and rapid recombination of photogenerated electron-hole pairs still existed [11-12]. In order to overcome these problems of CeO_2 , researchers have proposed many modification methods, the heterojunction strategy was one of the more useful ways [13-14]. For example, Kaur et al used MOF material DUT-8 (Zn/Ni) based on Ni and Zn to form heterojunction composites with CeO_2 to degrade dichlorophenol, and its degradation efficiency was higher than that of pure components [15]. Silver phosphate (Ag_3PO_4) could exhibit strong oxidation ability in the wavelength range of 300-530 nm. Among them, it has been widely studied in the degradation of organic pollutants in water. However, Ag_3PO_4 had poor stability and photocorrosion in the photocatalytic process [16], which had a negative impact on the catalytic efficiency of the material. The excellent quantum efficiency of Ag_3PO_4 made it suitable for the construction of various heterojunction photocatalytic system materials, especially for the degradation of organic pollutants [17]. At present, the photocatalytic and antibacterial properties of other semiconductors could be improved by loading Ag_3PO_4 [18-19]. For example, Ren et al added 10% mass Ag_3PO_4 to construct a double Z-scheme $\text{BiVO}_4/\text{g-C}_3\text{N}_4/\text{Ag}_3\text{PO}_4$ heterojunction composite to accelerate its catalytic and inhibitory effects on *E. coli* and *S. aureus* [20].

Based on the cost-effective inorganic photocatalytic material CeO_2 , $\text{Ag}_3\text{PO}_4/\text{CeO}_2$ composites were prepared by using Ag_3PO_4 with relatively excellent photocatalytic and antibacterial properties of traditional inorganic photocatalytic materials, and the adsorption and degradation effects on Rhodamine B and antibacterial effects on *E. coli* were actively explored.

2. Experimental

2.1. Preparation of $\text{Ag}_3\text{PO}_4/\text{CeO}_2$

Preparation of CeO_2 : A certain amount of $\text{Ce}(\text{NO}_3)_3 \cdot 6\text{H}_2\text{O}$ was dissolved in deionized water, and a certain amount of 1,3,5-benzenetricarboxylic acid was dissolved in water-ethanol ($V_{\text{water}} : V_{\text{ethanol}} = 1:1$) solution. Then the aqueous solution of $\text{Ce}(\text{NO}_3)_3 \cdot 6\text{H}_2\text{O}$ was dripped into 1,3,5-benzenetricarboxylic acid water-ethanol solution, and hold it in water bath at 60°C for 1 h with magnetic stirring. After centrifugation, the obtained precipitate was washed with deionized water

and methanol successively, dried at 80°C and calcined at 700°C for 8h in a muffle furnace.

Preparation of Ag_3PO_4 : 20 mL 0.15mol/L AgNO_3 DMF/ H_2O solution ($V_{\text{DMF}} : V_{\text{water}} = 5 : 15$) was prepared and stirred for 10min at 35°C with a magnetic stirrer. Then 10 mL 0.45mol/L Na_2HPO_4 solution was added drop by drop and stirred for 1 h. After centrifugation, the obtained yellow precipitate was washed with pure water and anhydrous ethanol alternately for 2 ~ 3 times, and dried in a vacuum drying oven at 60°C.

Preparation of $\text{Ag}_3\text{PO}_4/\text{CeO}_2$ composite: 20 mL 0.15mol/L AgNO_3 DMF/ H_2O solution ($V_{\text{DMF}} : V_{\text{water}} = 5 : 15$) was prepared and stirred for 10 min at 35°C with a magnetic stirrer. 0.1045 g CeO_2 was added, and continued to stir for 30 min, and then added 10 mL 0.45 mol/L Na_2HPO_4 solution drop by drop for 1 h. After Centrifugation, the obtained product was washed with pure water, ethanol alternately. The preparation rout of $\text{Ag}_3\text{PO}_4/\text{CeO}_2$ composite was shown in Fig. 1.

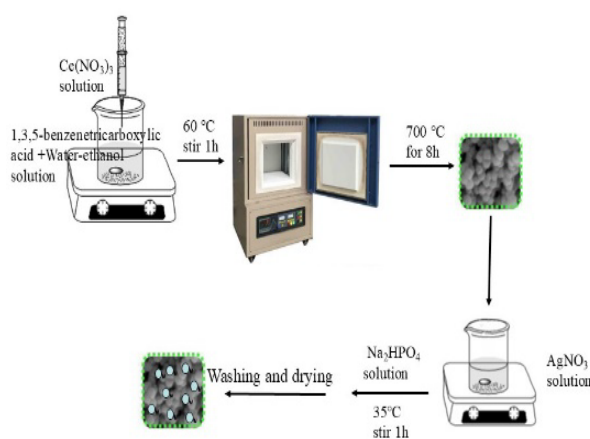


Fig. 1. Preparation route of $\text{Ag}_3\text{PO}_4 / \text{CeO}_2$.

2.2. Photocatalysis experiment

0.1g of the prepared sample was used for adsorption degradation of 30 mL 40 mg/L Rhodamine B solution. The initial absorbance was measured, and then 2 mL of supernatant was moved to measure UV-visible absorbance at $\lambda=554$ nm every 0.5h until the end of 2.5 h illumination. Degradation rate was calculated in formula (1).

$$D\% = \frac{C_0 - C_t}{C_0} = \frac{A_0 - A_t}{A_0} \times 100\% \quad (1)$$

2.3. Antibacterial experiment

Growth inhibition curve experiment : 10 mL beef extract peptone liquid medium was taken, and 100 μL of properly diluted E.coli bacterial solution was added and shaken well. 1 mL CeO_2 suspension solution (or Ag_3PO_4 or $\text{Ag}_3\text{PO}_4/\text{CeO}_2$ suspension solution) with a concentration of 80 mg /L was added. The shaking culture was carried out at 37°C, 140 r/min. The beef extract peptone liquid medium was used as the blank, and the absorbance at 625 nm was measured by ultraviolet-visible spectrophotometer. The absorbance was measured every 2 h until 24 h.

Colony number experiment : 400 μL 10^6 CFU/mL E.coli bacterial solution was taken and 100 μL 80 mg/L $\text{Ag}_3\text{PO}_4/\text{CeO}_2$ (CeO_2 or Ag_3PO_4) suspension was added. In the control group, 100 μL sterile water was added and fully shaken. 100 μL bacterial droplets were taken on the plate and coated with a coating device. The cells were cultured at 37 °C for 24 h. At last the colony growth of the plate was observed.

Bacteriostatic zone test: At first, the activated E. coli was diluted appropriately, and the medium was poured into a dish. Secondly 100 μL diluted bacterial solution was spread it evenly with a coater. Then the filter paper which was fully soaked 10 μL of the corresponding material suspension was placed on the surface of the medium. After incubate at 37°C for 20 h, the bacteriostatic zone was observed at last.

SEM of E. coli by antibacterial experiment: 1mL of $\text{Ag}_3\text{PO}_4/\text{CeO}_2$ composite particle suspension with a concentration of 80mg/L was added to the experimental group of E. coli's solution, and 1mL of sterile water was added as the control group. Then the bacteria solution was continued to incubate at 37°C for 5 h. After centrifugation, 8ml of each upper solution was absorbed, and the bacteria were collected. The bacteria were washed with 10mL PBS buffer and centrifuged with high speed refrigerated for 5 min. After centrifugation, PBS buffer was discarded and 2.5% glutaraldehyde fixing solution was added to the centrifuge tube and hold it overnight in a refrigerator at 4°C. After centrifuge, the gradient dehydration was performed on thallus with 30%, 50%, 70%, 90%, 100% ethanol aqueous solution. At last, after freeze-drying, the cells were sprayed with gold, and their morphology was observed by by scanning electron microscope.

2.4. Characterization of composites

X-ray powder diffraction pattern (XRD) was obtained by a D/ Max 3B X-ray diffractometer (Japan) with Cu K α irradiation source ($\lambda=1.5418$ Å) through the 2θ range from 5° to 90. The optical properties of the samples were characterized by a UV-2600 ultraviolet/visible diffuse reflectance spectrophotometer (DRS). The concentration of organic simulated dyes was obtained by UV-Vis Spectrophotometer (model: 8453, Agilent, USA). Field Emission Environment Scanning Electron Microscope (FEI Quanta 200FEG, Dutch Philips) was used to test the morphologies of E. coli.

3. Results and discussion

3.1. Characterization of composites

3.1.1. XRD characterization of $\text{Ag}_3\text{PO}_4/\text{CeO}_2$ composites

XRD spectra of $\text{Ag}_3\text{PO}_4/\text{CeO}_2$ composites was shown in Fig.2. It could be seen that the 2θ at 28.61°, 33.06°, 47.51°, 56.14°, 59.14°, 69.35° and 76.63 °, corresponding to crystal faces (111), (200), (220), (311), (222), (400) and (331) of cubic fluorite structure of CeO_2 (PDF # 34-0394). While, a series of diffraction peaks were shown at 2θ at 20.93°, 29.72°, 33.26°, 36.59°, 42.35°, 47.82°, 52.10 °, 55.10°, 57.42°, 61.77°, 71.97° and 87.25°, which were almost completely matched with the Ag_3PO_4 standard card (PDF # 06-0505). The overall peak shape of XRD of $\text{Ag}_3\text{PO}_4/\text{CeO}_2$ was sharp, indicating that the crystallinity of the sample was relatively high and the crystal form was good.

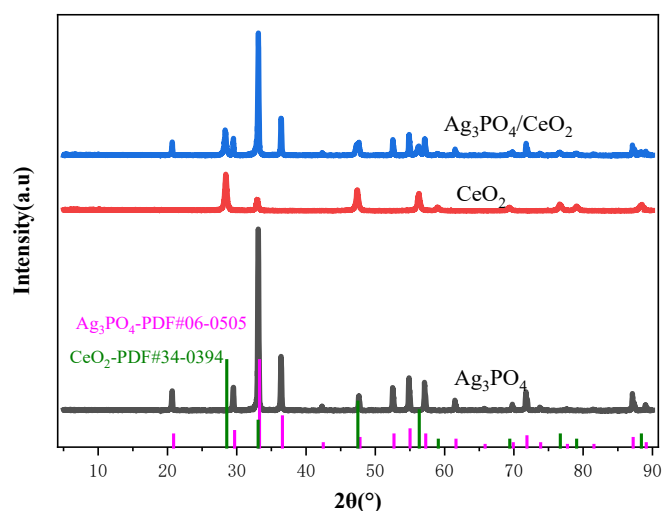


Fig. 2. XRD spectra of Ag_3PO_4/CeO_2 .

3.1.2. UV-Vis DRS characterization of Ag_3PO_4/CeO_2 composites

The UV-Vis absorption spectrum of Ag_3PO_4/CeO_2 was shown in Fig. 3(a). It showed that CeO_2 had the weakest light response. After 400nm (visible light), the spectral response of CeO_2 , Ag_3PO_4/CeO_2 and Ag_3PO_4 catalysts was enhanced successively. The curve of $(\alpha h\nu)^2$ vs. $h\nu$ was shown in Fig.3(b). Through the fitting analysis of the curve $(\alpha h\nu)^2$ vs. $h\nu$, it was calculated that the optical band gap of Ag_3PO_4 and CeO_2 was 1.81 and 2.28 respectively, and the optical band gap of Ag_3PO_4/CeO_2 was 1.96eV, which was between CeO_2 and Ag_3PO_4 . It could be seen that the band gap energy (E_g) of Ag_3PO_4/CeO_2 composite material was reduced by 0.32eV compared with pure CeO_2 material, which mean that the light energy required for the electron transition from valence band to conduction band of Ag_3PO_4/CeO_2 material was reduced, and the introduction of Ag_3PO_4 effectively inhibited the recombination of photogenerated electron-hole pairs and produced more active photogenerated electron-hole pairs, which was conducive to the improvement of photocatalytic activity.

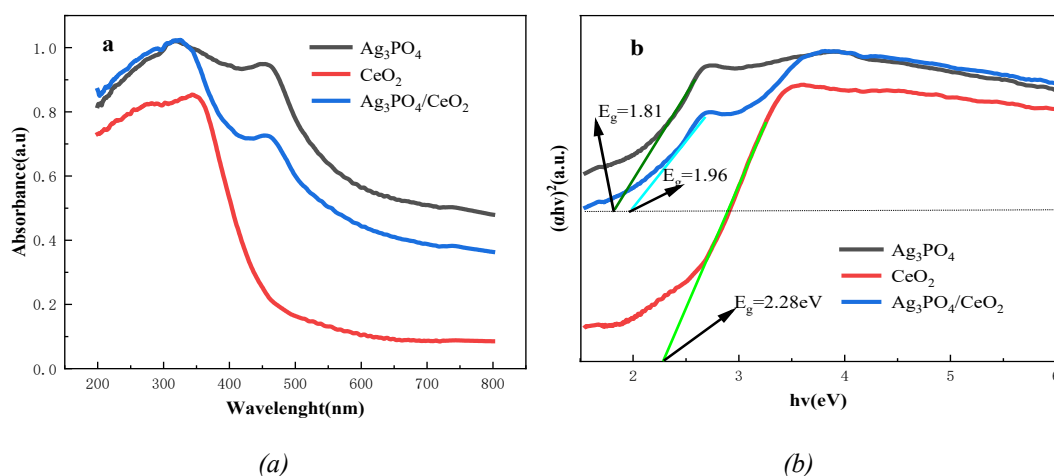


Fig. 3. (a) UV-Vis absorption spectra of Ag_3PO_4/CeO_2 composites, and (b) $(\alpha h\nu)^2$ vs. $h\nu$ curves.

3.2. Photocatalytic properties of Ag_3PO_4/CeO_2 composites

The degradation of Rhodamine B by Ag_3PO_4/CeO_2 composite was shown in Fig. 4. It could be seen from the figure that the degradation effect of each material on Rhodamine B gradually increased with time. The degradation rates of CeO_2 , Ag_3PO_4 and Ag_3PO_4/CeO_2 were 5.83 %, 11.67 % and 12.34 %, respectively after 0.5 h in dark room. The degradation rates were 15.74 %, 59.60 % and 99.91 %, respectively after 2.5 h in visible light. The results showed that the degradation rate of Ag_3PO_4/CeO_2 was 6.34 times and 1.67 times higher than that of pure CeO_2 and pure Ag_3PO_4 . According to the UV-Vis DRS characterization data of 3.1.2 and the experimental data of 3.4 effect of quencher on degradation of Rhodamine B, the improvement of the degradation efficiency of Ag_3PO_4/CeO_2 was mainly due to the introduction of Ag_3PO_4 , which reduced the band gap energy of the material system, facilitated the excitation of electron-hole pairs, increasing h^+ and $\cdot O_2^-$ radicals, and accelerating the degradation of organic simulants.

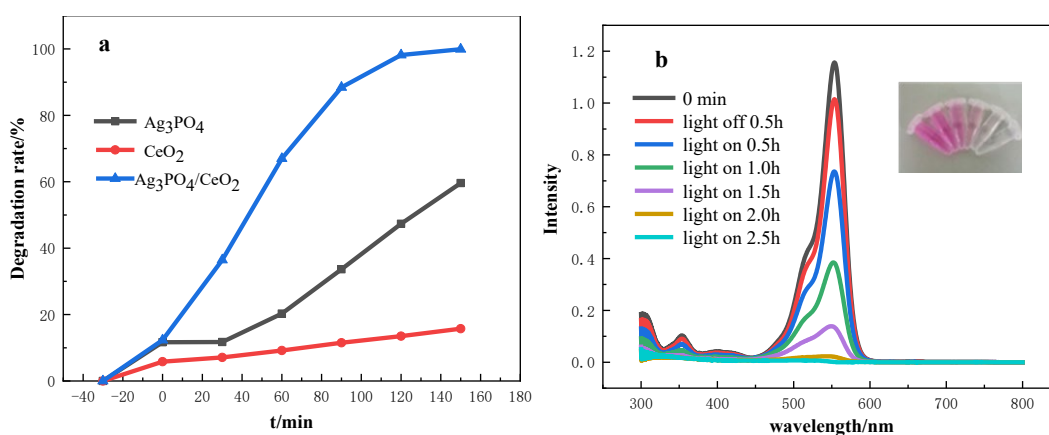


Fig. 4. Degradation diagram of Rhodamine B by Ag_3PO_4/CeO_2 composites (a: degradation rate-time diagram; b: Ultraviolet-visible spectrum of Rhodamine B during degradation by Ag_3PO_4/CeO_2).

3.3. Antibacterial capability of Ag_3PO_4/CeO_2 composites

Data of relevant bacteriostasis experiments was shown in Fig.5-Fig.8. From the growth curve, colony number experiment and inhibition zone experiment of *E. coli*, CeO_2 had a weak inhibitory effect on *E. coli*. Ag_3PO_4 and Ag_3PO_4/CeO_2 had a certain antibacterial effect on *E. coli*, and the order of antibacterial effect from strong to weak was: $Ag_3PO_4/CeO_2 > Ag_3PO_4 > CeO_2$. From the data of the conductivity of the *E. coli* bacterial liquid, it could be seen that the conductivity of the bacterial liquid centrifugal liquid increased with the increase of time. The order of conductivity of *E. coli* liquid was: $Ag_3PO_4/CeO_2 > Ag_3PO_4 > CeO_2 > \text{blank control group}$. The results of SEM of *E. coli* in the blank group and feeding Ag_3PO_4/CeO_2 showed that the morphology of *E. coli* in the blank group was fuller, while the morphology of *E. coli* with Ag_3PO_4/CeO_2 material was more concave. Combined with SEM and bacterial conductivity data, it speculated that the addition of composite particles to the bacterial solution could destroy the integrity of the cell wall. When the cell membrane of the bacteria was damaged, the integrity of the cell membrane was destroyed, and the intracellular substances would flow out of the body, which would increase the conductivity of the solution, collapse the cell body, and then cause the bacteria to die.

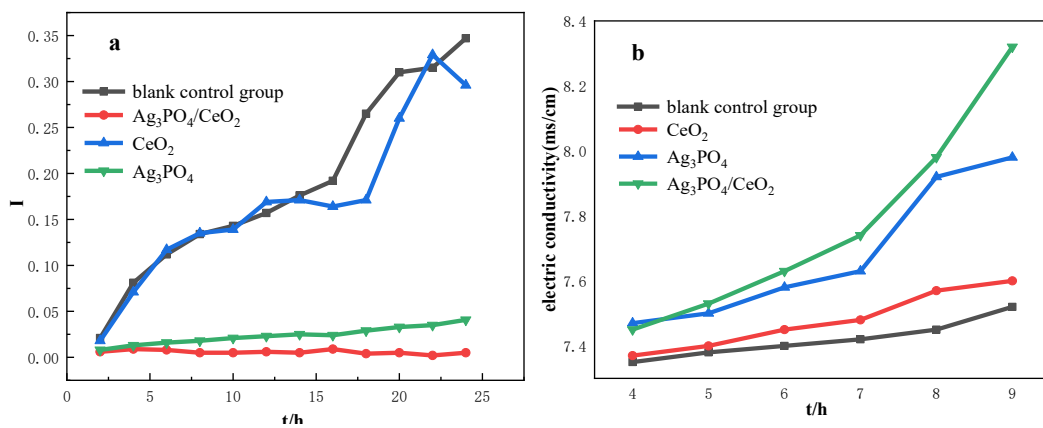


Fig. 5. (a) The growth inhibition curve of Ag_3PO_4/CeO_2 against *E. coli*; (b) the effect of feeding Ag_3PO_4/CeO_2 on the conductivity of *E. coli* solution.



Fig. 6. Three parallel data of the inhibition zone of Ag_3PO_4/CeO_2 against *E. coli* (the upper left corner of the plate was blank control sample, followed by Ag_3PO_4/CeO_2 , CeO_2 , Ag_3PO_4 clockwise).

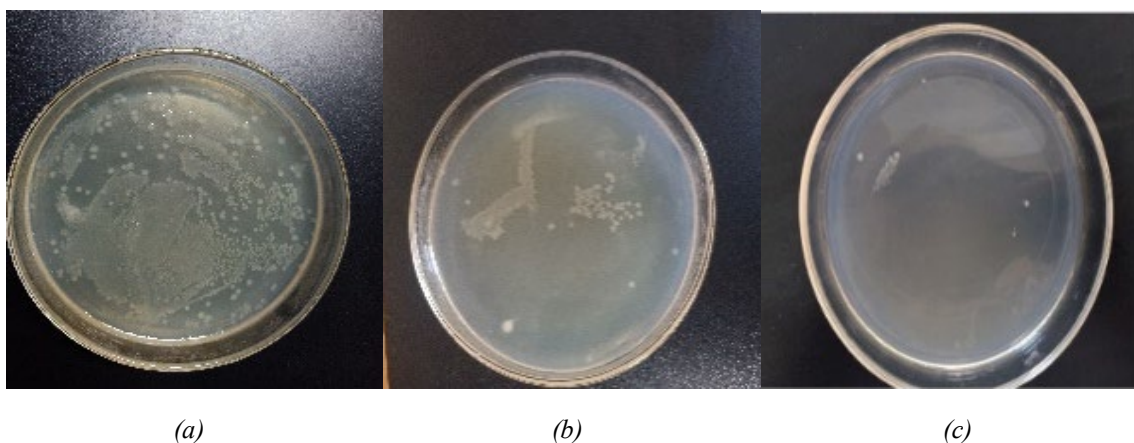


Fig. 7. Data of the number of colonies of *E. coli* by feeding materials (a: CeO_2 ; b: Ag_3PO_4 ; c: Ag_3PO_4/CeO_2).

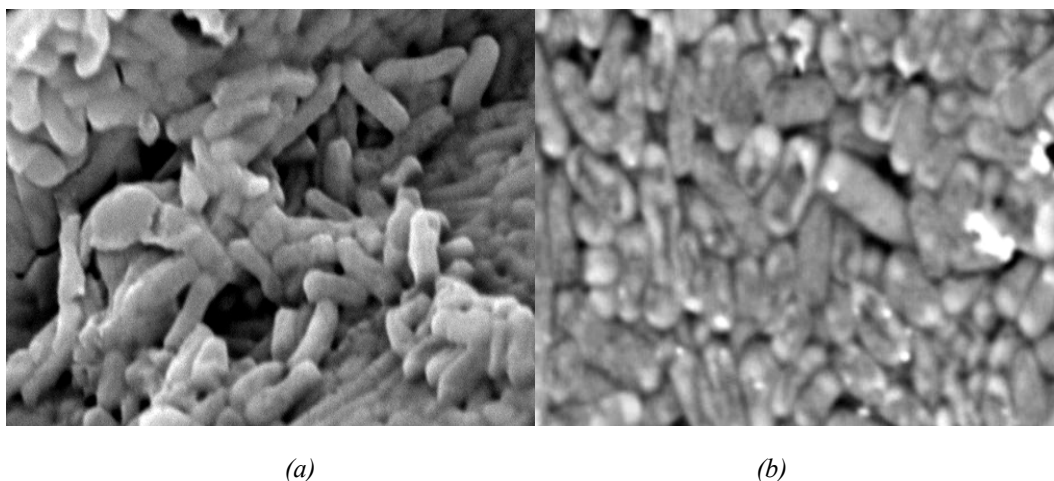


Fig. 8. SEM of *E. coli* (a) *E. coli* blank group (b) *E. coli* feeding ($\text{Ag}_3\text{PO}_4/\text{CeO}_2$) experimental group.

3.4. Photocatalytic and antibacterial mechanism of $\text{Ag}_3\text{PO}_4/\text{CeO}_2$ composites

In order to further study the effect of free radicals on the degradation of Rhodamine B in the process of photocatalytic degradation and the photocatalytic mechanism, the free radical capture experiment was carried out. As shown in Fig.9 (a), when the concentration of quencher was 0.075 mol/L, the photocatalytic degradation rates of Rhodamine B solution by $\text{Ag}_3\text{PO}_4/\text{CeO}_2$ with blank, sodium oxalate (h^+ quencher), dimethyl sulfoxide (e^- quencher), p-benzoquinone ($\cdot\text{O}_2^-$ quencher) and isopropanol ($\cdot\text{OH}$ quencher) were 99.02 %, 40.09 %, 95.86 %, 62.77 % and 98.42 %, respectively. The order of degradation efficiency was: blank > isopropanol > dimethyl sulfoxide > p-benzoquinone > sodium oxalate. It showed that the order of free radical participation in the reaction process was $\text{h}^+ > \cdot\text{O}_2^- > \text{e}^- > \cdot\text{OH}$. These data indicated that h^+ and $\cdot\text{O}_2^-$ are the main active substances in the photocatalytic process of $\text{Ag}_3\text{PO}_4/\text{CeO}_2$.

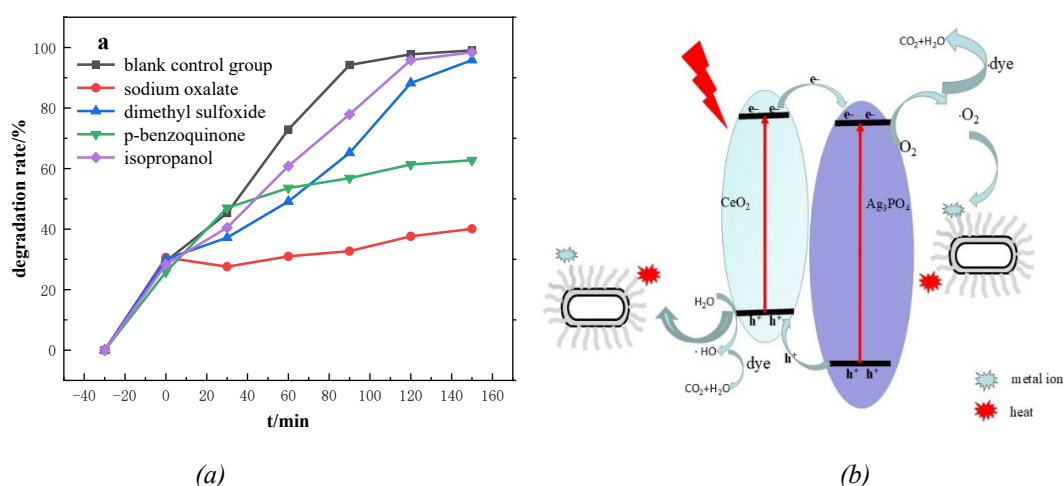


Fig. 9. (a) Effect of quencher on degradation of Rhodamine B by $\text{Ag}_3\text{PO}_4/\text{CeO}_2$; (b) The antibacterial mechanism diagram of $\text{Ag}_3\text{PO}_4/\text{CeO}_2$ photocatalytic.

The degradation mechanism of $\text{Ag}_3\text{PO}_4/\text{CeO}_2$ was shown in Fig.9 (b), under light irradiation, the electrons on the valence band of $\text{Ag}_3\text{PO}_4/\text{CeO}_2$ were excited to the conduction band to form the corresponding h^+ and e^- , and e^- combined with O_2 to form $\cdot\text{O}_2^-$. These active radicals further oxidized small molecules of organic dyes to form CO_2 and H_2O .

Combined with the conductivity experiment of bacterial solution and the SEM of bacteria on feeding, the antibacterial effect of $\text{Ag}_3\text{PO}_4/\text{CeO}_2$ material was mainly due to the fact that the material could produce active free radicals h^+ and $\cdot\text{O}_2^-$ and Ag^+ and corresponding $\text{Ce}^{3+}/\text{Ce}^{4+}$ and other metal ions [12,20-21], and released them to attack the cell membrane of *E. coli*, resulting in leakage of intracellular substances such as protein and DNA, resulting in apoptosis of cells.

4. Conclusion

$\text{Ag}_3\text{PO}_4/\text{CeO}_2$ composites were synthesized by loading Ag source on CeO_2 which was prepared by calcination method. The structure of $\text{Ag}_3\text{PO}_4/\text{CeO}_2$ composites was characterized by XRD and DRS. At the same time, the degradation effect of the material on the simulated organic Rhodamine B and the antibacterial effect of the material on *E. coli* were investigated by antibacterial growth curve, colony number and other experiments. The experimental results showed that the peak shape of $\text{Ag}_3\text{PO}_4/\text{CeO}_2$ was sharp and the crystal form was good. The band gap energy of $\text{Ag}_3\text{PO}_4/\text{CeO}_2$ was 1.93 eV which was lower than that of the main material CeO_2 (2.28 eV). The degradation rate of 30 mL 40 mg/L Rhodamine B solution by $\text{Ag}_3\text{PO}_4/\text{CeO}_2$ composite was 99.91 %, which was 6.34 times and 1.67 times that of pure CeO_2 and Ag_3PO_4 , respectively.

Combined with relevant bacteriostatic experimental data, the order of antibacterial activity of different substances was: $\text{Ag}_3\text{PO}_4/\text{CeO}_2 > \text{Ag}_3\text{PO}_4 > \text{CeO}_2$. And also it was found that the order of free radical generation from large to small in the reaction process was $\text{h}^+ > \cdot\text{O}_2^- > \text{e}^- > \cdot\text{OH}$, and h^+ and $\cdot\text{O}_2^-$ were mainly produced in the photodegradation process. Combined with its physical and chemical properties, $\text{Ag}_3\text{PO}_4/\text{CeO}_2$ photocatalytic materials may produce reactive oxygen species (ROS) and corresponding metal ions during the antibacterial process, and released them to attack the cell wall of *E. coli*, thereby leading to cytoplasmic leakage and cell apoptosis.

Acknowledgements

The work was supported by Guangxi Provincial Natural Science Foundation of China (2024GXNSFBA010433); university-level scientific research project of Hechi University (2023XJZD004); Innovation and entrepreneurship training program for college students (S202310605003).

References

- [1] Y. Wu, Y. Yang, Y. Liu, L. Zhang, L. Feng, *Chemical Engineering Journal*, 358, 332-1341 (2019); <https://doi.org/10.1016/j.cej.2018.10.125>
- [2] J. J. Rueda-Marquez, I. Levchuk, P. F. Ibanez, M. Sillanpaa, *J. Clean. Prod.*, 258,

- 120694(2020); <https://doi.org/10.1016/j.jclepro.2020.120694>
- [3] D. H. Amin, A. Abolmaaty, Bulletin of the National Research Centre, 44(1), 172(2020); <https://doi.org/10.1186/s42269-020-00423-8>
- [4] M. Alavi, N. Karimi, T. Valadbeigi, ACS Biomaterials Science & Engineering, 5, 4228-4243(2019); <https://doi.10.1021/acsbiomaterials.9b00274>
- [5] D. Adeyemi, A. Adeluola, M. Akinbile, O. Johnson, G. Ayools, African Journal of Clinical and Experimental Microbiology, 21(2), 106-113(2020); <https://doi.10.4314/ajcem.v21i2.4>
- [6] M. V. Lungu, E. Vasile, M. Lucaci, D. Pătroi , N. Mihăilescu, F. Grigore, V. Marinescu, A. Brătulescu , S. Mitrea, A. Sobetkii, A. Sobetkii, M. Popa , M. Chifiriuc , Materials Characterization, 120, 69-81(2016); <https://doi.org/10.1016/j.matchar.2016.08.022>
- [7] C. R. Kumar, V. Betageri, G. Nagaraju, G. H. Pujar, H. S. Onkarappa, M. S. Latha, Journal of Inorganic and Organometallic Polymers and Materials, 30(9), 3410-3417(2020); <https://doi.org/10.1007/s10904-020-01507-8>
- [8] D. Tran, M. Pham, X. Bui, Y. Wang, S. You, Solar Energy, 240, 443-466(2022); <https://doi.org/10.1016/j.solener.2022.04.051>
- [9] S. N. Naidi, M. H. Harunsani, A. L. Tan, M. M. Khan, Journal of Materials Chemistry B, 9(28), 5599-5620(2021); <https://doi.10.1039/d1tb00248a>
- [10] M. Liang, T. Borjigin, Y. Zhang, B. Liu, H. Liu, H. Guo, Applied Catalysis B: Environmental, 243, 566-575(2019); <https://doi.org/10.1016/j.apcatb.2018.11.010>
- [11] B. Borjigin, L. Ding, H. Q. Li, X. J. Wang, Chemical Engineering Journal, 402, 126070(2020); <https://doi.org/10.1016/j.cej.2020.126070>
- [12] F. Chapari, M. Haghighi, E. Fatehifar, M. Shabani, N. Mikaeeli, Journal of Industrial and Engineering Chemistry, 116, 142-158 (2022); Journal of Industrial and Engineering Chemistry, 116, 142-158(2022); <https://doi.org/10.1016/j.jiec.2022.08.031>
- [13] H. H. Chen, S. H. Luo, X. F. Lei, F. Teng, X. B. Ji, X. D. Li, Transactions of Nonferrous Metals Society of China, 34, 1951-1964(2024); [https://doi.10.1016/S1003-6326\(24\)66518-0](https://doi.10.1016/S1003-6326(24)66518-0)
- [14] F. Chapari, M. Haghighi, E. Fatehifar, M. Shabanni, N. Mikaeeli, Journal of Industrial and Engineering Chemistry, 116, 142-158(2022); <https://doi.org/10.1016/j.jiec.2022.08.031>
- [15] G. D. Kaur, A. Sharma, D. Sud, R. Rai, Journal of Molecular Structure, 1319, 139417(2025); <https://doi.org/10.1016/j.molstruc.2024.139417>
- [16] Y. Li, X. Xiao, Z. Ye, Applied Surface Science, 467-468, 902-911(2019); <https://doi.org/10.1016/j.apsusc.2018.10.226>
- [17] X. Chen, Y. Dai, X. Wang, J. Alloys Compd., 649, 910-932(2015); <https://doi.org/10.1016/j.jallcom.2015.07.174>
- [18] J. L. Liu, Y. X. Yi, K. T. Zhang, J. Liu, Y. Bao, J. Q. Li, H. Liu, Ceramics International, 50, 31051-31059(2024); <https://doi.org/10.1016/j.ceramint.2024.05.410>
- [19] L. Trindade, M. Assis, J. C. Souza, Al. Trench, Y. Rosa, M. Teodoro, A. Schwanke, E. Longo, F. Perrechil, A. R. C. Braga, Journal of Alloys and Compounds, 971, 172556(2024); <https://doi.org/10.1016/j.jallcom.2023.172556>
- [20] H. X. Ren, Z. Gong, M. Y. Zhang, Y. H. Liu, Y. G. LV, Chemical Physics Letters, 85, 141738(2024); <https://doi.org/10.1016/j.cplett.2024.141738>
- [21] B. G. Ye, Z. W. Zhao, H. G. Liu, Journal of Molecular Structure, 1272, 134205(2023); <https://doi.org/10.1016/j.molstruc.2022.134205>